Gao, Hanming et al.

Article

Experimental study of a mesoscale combustor-powered thermoelectric generator

Energy Reports

Provided in Cooperation with:
Elsevier

Suggested Citation: Gao, Hanming et al. (2020) : Experimental study of a mesoscale combustor-powered thermoelectric generator, Energy Reports, ISSN 2352-4847, Elsevier, Amsterdam, Vol. 6, pp. 507-517,
https://doi.org/10.1016/j.egyr.2020.02.016

This Version is available at:
https://hdl.handle.net/10419/244053

Energy Reports 6 (2020) 507–517

Contents lists available at ScienceDirect

Energy Reports

journal homepage: www.elsevier.com/locate/egyr

Research paper

Experimental study of a mesoscale combustor-powered thermoelectric generator

Hanming Gao [a], Guoneng Li [b,*], Wei Ji [a], Dongya Zhu [b], Youqu Zheng [b], Feixing Ye [a], Wenwen Guo [b]

[a] Zhejiang Fuxing Shipping Co., Ltd., Hangzhou 310023, China
[b] Department of Energy and Environment System Engineering, Zhejiang University of Science and Technology, Hangzhou 310023, China

ARTICLE INFO

Article history:
Received 4 September 2019
Received in revised form 17 January 2020
Accepted 19 February 2020
Available online xxxx

Keywords:
Mesoscale combustor-powered thermoelectric generator
Heat collection efficiency
Residence time

ABSTRACT

Small-scale power sources should be developed with the rapid development of portable electronic equipments. This study presents a mesoscale combustor-powered thermoelectric generator (MCP-TEG). The MCP-TEG generates an electric power of 1.88 W with an overall efficiency of 1.74% at a substantial low hot-end temperature of 95 °C. The relationship among overall, combustion, heat collection and thermoelectric (TE) efficiencies was firstly established in this work. Detailed analysis reveals that the gap between the overall and TE efficiencies is mainly determined by combustion and heat collection efficiencies, and heat collection efficiency is closely related to the residence time of flue gases and preheating design of reactants. The obtained heat collection efficiency is larger than 77.4%, which augments the ratio of overall efficiency to TE efficiency reaching 75.3%, indicating that the present MCP-TEG is well designed. The state of the art of MCP-TEGs is partially revealed, indicating that the ratio of overall efficiency to TE efficiency is an effective metrics to evaluate the performance of various MCP-TEGs.

1. Introduction

Rapid development of portable electronic equipment such as mobile phones, laptops, and wearable medical devices, has stimulated the R&D of small-scale power sources. The essential stimulus is the higher energy density of hydrocarbons compared with rechargeable batteries. For example, the energy density of methane is 15,416 Wh/kg, which is much higher than the energy density of lithium battery (200–300 Wh/kg). This condition implies that methane provides 5 times higher energy density than lithium battery at 10% energy conversion efficiency. In addition, batteries have inherent disadvantages, such as long recharging time, limited life, and adverse environmental impacts. Less than 3% of lithium batteries were recycled, and the rest were landfilled (Sonoc et al., 2015). Thus, hydrocarbon-powered micro/mesoscale power systems have attracted substantial interest, which are addressed in existing studies.

Micro gas turbines (Xiao et al., 2017), fuel cells (Zhang et al., 2018), thermophotovoltaic (TPV) generators (Mustafa et al., 2017), and thermoelectric generators (TEGs) (Mustafa et al., 2017) have been used as micro/mesoscale power systems. Although micro gas turbines and fuel cells perform efficiently, their maintenance hinders their application. These problems include high-speed rotating parts, high-temperature bearing, and noises for micro gas turbines, and humidification, hydrogen storage, and safety for fuel cells. TPV generators and TEGs are straightforward systems and subjected to low maintenance because of their small moving parts. However, TPV generators and TEGs have limited conversion efficiency. Material revolution has accelerated in the past few years, creating excellent TE (Zhao et al., 2014c) and PV materials (Essig et al., 2016). Thus, existing studies on TPV generator and TEGs are indispensable.

A micro/mesoscale combustor-powered TEG (MCP-TEG) was investigated in the present work. An MCP-TEG utilizes the Seebeck effect, which converts temperature difference into electrical energy. Thus, the MCP-TEG is a promising solution for portable power sources. A brief literature review on MCP-TEGs is provided in the following section. Detail performance of these reported studies (Vican et al., 2002; Norton et al., 2005; Federici et al., 2006; Yoshida et al., 2006; Karim et al., 2008; Jiang et al., 2011; Marton et al., 2011; Shimokuri et al., 2015; Yadav et al., 2015; Singh et al., 2016; Merotto et al., 2016; Shimokuri et al., 2017; Abedi et al., 2017; Aravind et al., 2018b,a; Fanciulli et al., 2018; Aravind et al., 2019; Guggilla et al., 2019) are shown in Table 1, where η_{fuel}, η_{heat} and η_{sys} are combustion, heat collection and overall efficiencies, respectively.

Researchers made great efforts to generate a watt of electric power with their MCP-TEGs before the year of 2010. Vican

* Corresponding author.
E-mail address: 109026@zust.edu.cn (G. Li).

https://doi.org/10.1016/j.egyr.2020.02.016

Nomenclature

A_{flue}	Cross sectional area of flue gas channel (m^2)
A_{surf}	Outside surface area of insulation (m^2)
c_p	Heat capacity (kJ/kg K)
h_{air}	Convective heat transfer coefficient (W/m^2 K)
k	Thermal conductivity (W/m K)
L	Length of thermoelectric leg (m)
L_{flue}	Length of flue gas channel (m)
m_{flue}	Mass flow rate of flue gases (kg/s)
m_{fuel}	Fuel mass flow rate (kg/s)
m_{burnt}	Combusted fuel mass flow rate (kg/s)
n	Electrical resistivity ratio (m)
P	Electric power (W)
P_{conv}	Heat loss rate through convections (W)
P_{flue}	Heat flow rate of flue gases (W)
P_{in}	Input power (W)
P_{ld}	Load power (W)
P_{max}	Maximum electricity power (W)
P_{rad}	Heat loss rate through thermal radiations (W)
P_{TE}	Heat power through TE modules (W)
Q_{flue}	Volume flow rate (m^3/s)
r	Thermal contact ratio (dimensionless)
R_{ld}	Load resistance (Ω)
T	Temperature (°C)
T_{ave}	Average temperature, $(T_h + T_c)/2$ (°C)
T_c	Cold-end temperature (°C)
T_f	Combustion temperature (°C)
T_h	Hot-end temperature (°C)
T_{in}	Inlet air temperature (°C)
T_{out}	Flue gas temperature (°C)
T_{surf}	Outside surface temperature of insulation (°C)
ΔT	Temperature difference (°C), $\Delta T = T_h - T_c$
U	Voltage (V)
w	Ratio of ceramic thickness to thermoelectric leg (dimensionless)
Z	Thermoelectric figure-of-merit (1/K)
α	Seebeck coefficient (V/K)
ρ	Electrical resistivity (Ω m)
φ	Equivalent ratio (dimensionless)
ε	Emissivity (dimensionless)
τ	Residence time (ms)
σ	Stefan–Boltzmann constant (W/m^2 K^4)
η_{fuel}	Combustion efficiency (%)
η_{heat}	Heat collection efficiency (%)
η_{sys}	Overall efficiency (%)
η_{TE}	TE efficiency (%)
ξ_{heat}	Heat loss ratio (%)

Abbreviations

CTC	Catalytic combustion
DAQ	Data acquisition
DTC	Direct combustion
IR	Infrared
MFC	Mass flow rate controller
SLPM	Standard liter per minute
TE	Thermoelectric
TEG	TE generator
TPV	Thermophotovoltaic
MCP-TEG	Micro/mesoscale combustor-powered TEG

et al. (2002) from Princeton University presented an MCP-TEG. An electric power of 0.052 W was obtained, and the corresponding overall efficiency was 0.57%. Several researchers (Norton et al., 2005; Federici et al., 2006; Karim et al., 2008) from University of Delaware designed several MCP-TEGs. The catalytic fuel combustions in these studies (Norton et al., 2005; Federici et al., 2006; Karim et al., 2008) were approximately complete. The maximum electric power was 1 W (Norton et al., 2005), and the overall efficiency was 1.1% (Karim et al., 2008). A similar work was conducted by Yoshida et al. (2006). The electric power was 0.185 W due to the limited input power, and the overall efficiency was increased to 2.8%. Jiang et al. (2011) from Guangzhou Institute of Energy Conversion of China proposed another type of MCP-TEG in 2011, and successfully generated an electric power of 2 W with an overall efficiency of 1.25%. Their combustor worked without catalytic material, and directly ignited the fuel to maintain continuous combustion. Catalytic combustion has been applied in other studies. Marton et al. (2011) from Massachusetts Institute of Technology obtained an electric power of 5.82 at an overall efficiency of 2.53%. A new record of electric power (18.1 W) was reported in Shimokuri's studies from Hiroshima University (Shimokuri et al., 2015, 2017) in 2017. Their vortex burner augmented the overall efficiency to 3.01%. Researchers (Yadav et al., 2015; Aravind et al., 2018b,a, 2019) from Indian Institute of Technology Bombay conducted subsequent studies. They obtained higher overall efficiencies (>4.0%) in water-cooled MCP-TEGs (Yadav et al., 2015; Aravind et al., 2018b,a) compared with previous studies and high overall efficiency (2.5%) in their air-cooled MCP-TEGs (Aravind et al., 2019). Singh et al. (2016) from Cardiff University reported an overall efficiency of 1.42% and approximately complete fuel combustion. Catalytic combustion was optimized by several researchers (Merotto et al., 2016; Abedi et al., 2017, and Fanciulli et al., 2018) from National Research Council of Italy. Maximum electric power of 9.86 W was obtained (Merotto et al., 2016), and the overall efficiency varied between 1.1% (Fanciulli et al., 2018) and 2.85% (Merotto et al., 2016). Guggilla et al. (2019) from Rowan University proposed an MCP-TEG. They obtained good results but the overall efficiency was limited.

As previously discussed, MCP-TEGs burn gas/liquid fuels, and directly convert heat into electricity. Stove-powered TEGs by burning solid fuels have been extensively investigated by Nuwayhid et al. (2005), Najjar and Kseibi (2017), O'Shaughnessy et al. (2015), Champier et al. (2011), Montecucco et al. (2017), and Sornek et al. (2019). They presented different prototypes of stove-powered TEGs, which obtained electric power of 75.2 W (Sornek et al., 2019) and TE efficiency of 5% (Montecucco et al., 2017). A brief review on stove-powered TEGs can be found in our previous work (Li et al., 2018). Other energy harvesting systems including combustion powered piezoelectric generators (Zhao et al., 2014a; Zhao and Ega, 2014) and bladeless electromagnetic generators (Zhao et al., 2014b) are under development in recent years.

In the present work, an MCP-TEG was presented and evaluated in terms of heat collection efficiency to increase the overall

Table 1
Performance comparisons of various MCP-TEGs.

Authors	Year	T_h	ΔT	Efficiency (%)			P_{max} (W)	Reaction type[b]	Notes
				η_{heat}	η_{sys}	η_{fuel}			
Vican et al. (2002)	2002	115.5	92.5	–	0.57	100	0.052	CTC	
Norton et al. (2005)	2004	–	253	–	∼0.85	100	∼1	CTC	Case: H_2/air mixture at $\varphi = 1.0$
Federici et al. (2006)	2006	170	85	19.3	0.51	100	0.45	CTC	Case: 1.4 SLPM
Yoshida et al. (2006)	2006	125	70	30–44	2.8	99.5	0.185	CTC	[a]Data from different cases
Karim et al. (2008)	2008	–	160	–	1.1	100	0.65	CTC	
Jiang et al. (2011)	2011	200	130	–	1.25	100	2	DTC	
Marton et al. (2011)	2011	312	266	–	2.53	100	5.82	CTC	
Shimokuri et al. (2015)	2015	156	126	–	2.23	100	4.76	DTC	$\eta_{sys} = 2.36\%$ at $P_{max} = 8.1$ W
Yadav et al. (2015)	2015	250	–	–	4.6	–	2.35	DTC	
Singh et al. (2016)	2016	197	88	–	1.42	100	3.54	DTC	Case: 250 W input power
Merotto et al. (2016)	2016	258	200	–	2.36	96	9.86	CTC	$\eta_{sys} = 2.85\%$ at $P_{max} = 6.78$ W
Shimokuri et al. (2017)	2017	200	165	75.3	3.01	86.9	18.1	DTC	
Abedi et al. (2017)	2017	168	150	–	2.27	96.4	5.92	CTC	
Aravind et al. (2018b)	2018	130	99	34.4	4.03	–	3.89	DTC	[a]Data from different cases
Aravind et al. (2018a)	2018	150	115	33.5	4.66	–	4.52	DTC	[a]Data from different cases
Fanciulli et al. (2018)	2018	160	128	94	1.1	56	0.84	CTC	$\eta_{sys} = 1.4\%$ at $P_{max} = 0.6$ W
Aravind et al. (2019)	2019	221	124	25.7	2.5	–	2.4	DTC	Case: 10 m/s, Fin+Fan at 3000 rpm
Guggilla et al. (2019)	2019	140	62	–	0.1	70	0.49	CTC	
Present	2019	95	74	77.4	1.74	97.4	1.88	DTC	

- denotes not-found or not-studied.
[a]Denotes that a complete set of data cannot be found. Data from close cases were listed for comparison and discussion purpose. Certain uncertainties should be aware.
[b]CTC and DTC denote catalytic-combustion and direct-combustion, respectively.

efficiency while keeping the hot-end temperature lower than 100 °C. The MCP-TEG burned methane with designed input power between 72 W and 108 W, and produced a maximum electric power of 1.88 W. The corresponding overall efficiency was 1.74% at the hot-end temperature of 95 °C. The ratio of overall efficiency to TE efficiency reached 75.4%, which was higher than those in previous studies. Detailed comparisons and discussions on the experimental results with previous studies were presented.

2. Methodology

2.1. MCP-TEG configuration

The configuration of the proposed MCP-TEG is shown in Fig. 1. It was composed of a mesoscale combustor, two TE modules, and two water-cooled heat sinks. The mesoscale combustor was assembled with two copper plates featured by multiple notch grooves, and its overall dimensions were 40 mm × 40 mm × 16 mm. The combustion zone was located in the center of the copper plate. Fuel was injected through two 1 mm × 2 mm nozzles, and air was supplied through four 1 mm × 5 mm spouts. The channel hydraulic diameters of fuel, air, and flue gas were 2, 5.7 and 7.5 mm, respectively. The ratios of channel length to channel hydraulic diameter for fuel, air, and flue gas were 22, 10.9, and 14.9, respectively. This design increased the residence times of reactants and flue gases. The residence times of fuel, air, and flue gas were approximately 59, 78 and 60 ms respectively at the largest input power (108 W). The residence times for fuel and air were estimated based on inlet temperature (T_{in}), and the residence time for flue gas was calculated based on the average temperature between flue gas temperature (T_{out}) and combustion temperature (T_{f}). One TE module was sandwiched between the combustor and water-cooled heat sink. Thus, two TE modules and two water-cooled heat sinks were used in the MCP-TEG. Commercially available Bi_2Te_3-based TE modules, type "TEG1-12708" (SAGREON Co. Ltd., China) with dimensions of 40 mm × 40 mm × 3.3 mm, were utilized in the proposed MCP-TEG. Its performance from datasheets provided by the manufacturer indicated that it performs well compared with similar TE modules from different manufacturers. The TE module generates an electric power of 8.2 W at a temperature difference of 200 °C. Temperature-dependent properties of the TE material were used to theoretically calculate the TE efficiency. The water-cooled heat sink has M-shaped channels inside, and its dimensions are 40 mm × 40 mm × 12 mm. According to Chou's review (Chou et al., 2011) and Singh's work (Singh et al., 2016), the combustor was categorized as a microscale one when the burner dimension is in the magnitude of millimeter (less than 4 mm); while the combustor with a burner dimension in the magnitude of centimeter (∼2 cm) was classified as mesoscale. For a mesoscale combustor, the input power could be as high as a thousand watts, such as 600 W in Shimokuri's work (Shimokuri et al., 2017). Concerning that the burner dimensions in the present work are 13 mm × 6 mm × 5 mm, the combustor could be categorized as a mesoscale one.

2.2. Experimental setup

The experimental setup is shown in Fig. 2. Two Alicat mass flow controllers (MFCs) were used to supply methane and air. The accuracy of MFC is ±0.8% plus 0.1% of full scale (MFC for methane: 33.3 ml/s, MFC for air: 333.3 ml/s). Flue gas emissions (CO_2, CO, and NO) were measured with a Testo 340 gas analyzer. The accuracies of CO_2, CO and NO measurements are 0.2%vol., 10%vol., and 5 ppm, respectively. A thermocouple measuring combustion temperature is located in the combustion chamber, and two other thermocouples were located near the hot-end and cold-end sides of the TE module. Inlet air temperature and outlet flue gas temperature were also measured. The accuracy of thermocouples is 0.5%. The temperature signals were recorded with an Agilent-34970A data-acquisition (DAQ) instrument combined with a Benchlink Data Logger program. A Dali T8 infrared (IR) imager with 25 μm resolution was used to observe the temperature distribution of MCP-TEG and to estimate heat losses through convections and thermal radiations. Power load feature was measured with a Prodigit 3311F electronic load, and its measuring accuracy is ±0.5%. To keep the cold-end temperature low, a water pump, a radiator, and three blowers were used to dissipate heat from the cold-end of TE modules.

The input power in the present work were set to 72, 84, 96, and 108 W. These input powers were calculated by multiplying the mass flow rate of methane and the corresponding low heat value. The equivalent ratios were set to 0.9 and 1.0, and the fuel mass flow rate was kept constant when modifying the equivalent ratio. Errors of the measured parameters are listed in Table 2.

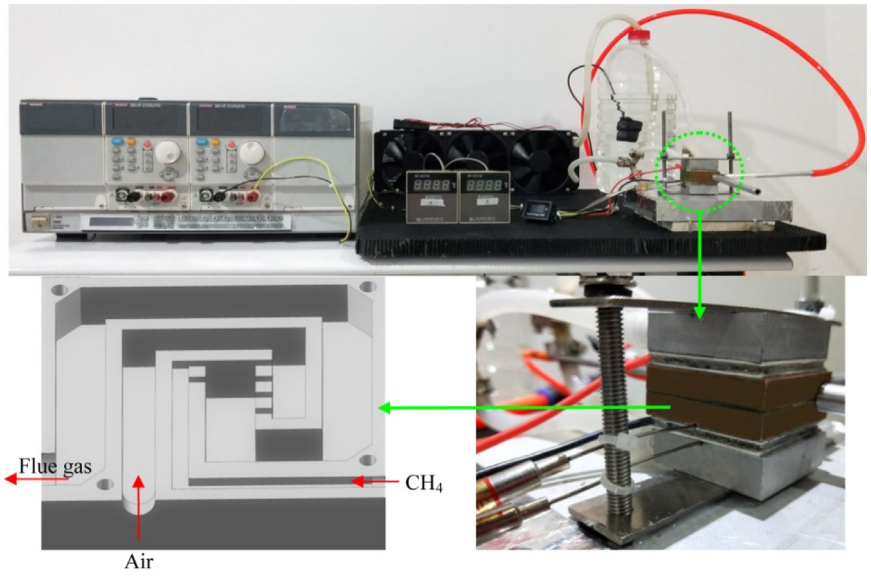

Fig. 1. Configuration of MCP-TEG.

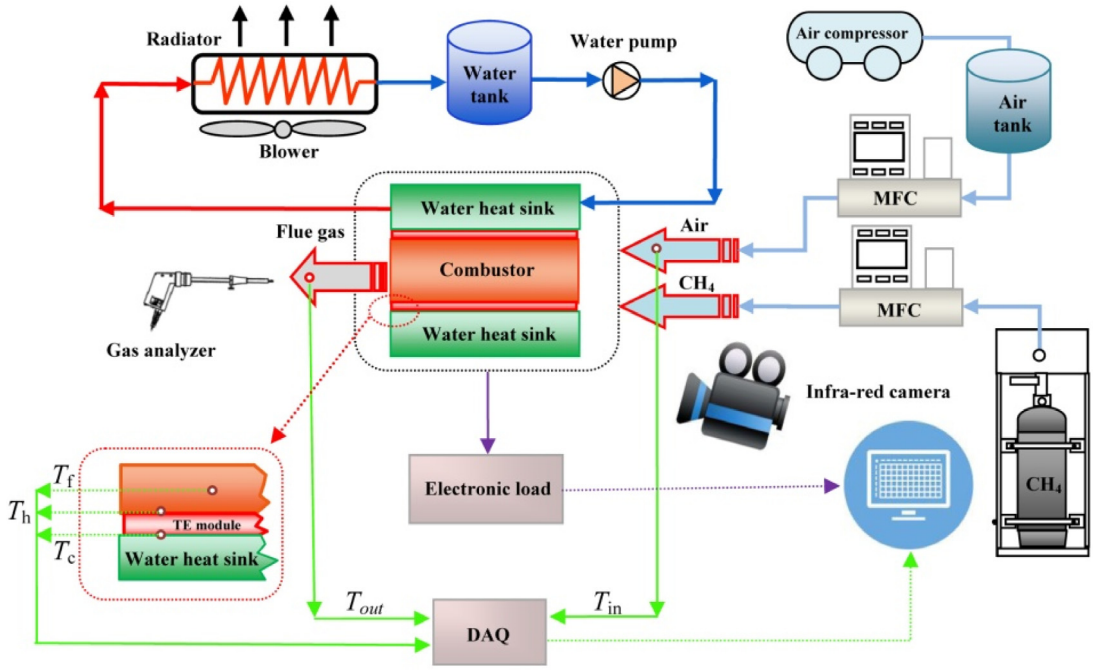

Fig. 2. Schematic of experimental setup.

Table 2
Errors of the measured parameters.

Parameter	Error	Parameter	Error
U (voltage)	±0.25%	P (electric power)	±0.5%
T (temperature)	±0.5%	m (mass flow rate)	±0.9%
CO_2	±0.2%	CO	±10 ppm
NO	±5 ppm	η_{fuel}	±1.1%
η_{heat}	±5.6%	η_{sys}	±1.4%

2.3. Parameter definitions

Fuel and air entered the combustor, and became flue gases through a chemical reaction (catalytic combustion or direct combustion). Combustion efficiency is defined as follows,

$$\eta_{\text{fuel}} = \frac{m_{\text{burnt}}}{m_{fuel}}, \tag{1}$$

where m_{fuel} and m_{burnt} are the fuel (CH_4) mass flow rate and combusted fuel flow rate, respectively. m_{burnt} can be obtained by measuring the CO_2 concentration in the flue gas without considering the CO concentration. This assumption was justified because CO concentration was low, which will be discussed in

Section 3.4. Thus, CH_4 oxidation can be expressed as,

$$CH_4 + 2O_2 \rightarrow CO_2 + 2H_2O(g). \quad (2)$$

This condition implies that CO_2 concentration is directly proportional to that of combusted CH_4 mass flow rate because no volume is created or vanished before and after the reaction. Meanwhile, heat is released through combustion, but only part of the heat can be collected and passed through TE modules. Thus, the heat collection efficiency is defined as follows,

$$\eta_{\text{heat}} = \frac{P_{TE}}{\eta_{\text{fuel}} P_{\text{in}}}, \quad (3)$$

where P_{in} is the input power. P_{TE} is the heat flow rate passing through the TE modules, which is difficult to be measured. P_{TE} is obtained by using the following equation.

$$P_{TE} = \eta_{\text{fuel}} P_{\text{in}} - P_{flue} - P_{conv} - P_{rad}, \quad (4)$$

where P_{flue}, P_{conv}, and P_{rad} are heat flow rate of flue gas, heat loss rate through natural convections, and heat loss rate through thermal radiations, respectively. The calculations of P_{flue}, P_{conv}, and P_{rad} will be discussed in Section 3.1. TE modules directly convert part of P_{TE} to electricity. Thus, TE efficiency, overall efficiency, and heat loss ratio can be defined as,

$$\eta_{\text{TE}} = \frac{P_{\max}}{P_{TE}}, \quad (5)$$

$$\eta_{\text{sys}} = \frac{P_{\max}}{P_{in}}, \quad (6)$$

$$\xi_{\text{heat}} = \frac{P_{\text{conv}} + P_{rad}}{P_{in}}. \quad (7)$$

where $P_{\max}$ represents the maximum electric power generated by TE modules. Thus, the overall efficiency should be less than the TE efficiency, and their relationship can be expressed as follows:

$$\eta_{\text{sys}} = \eta_{\text{fuel}} \eta_{\text{heat}} \eta_{\text{TE}}. \quad (8)$$

TE efficiency can be theoretically predicted as follows (Rowe, 1995; Rowe and Gao, 1998).

$$\eta_{TE} = \frac{T_{\text{h}} - T_{\text{c}}}{T_{\text{h}}} \left\{ (1 + 2rw)^2 \left[2 - 0.5 \left(\frac{T_{\text{h}} - T_{\text{c}}}{T_{\text{h}}} \right) + \left(\frac{4}{ZT_h} \right) \left(\frac{1 + n/L}{1 + 2rw} \right) \right] \right\}^{-1}, \quad (9)$$

where T_{h} and T_{c} are the hot-end and cold-end temperatures, respectively. The figure-of-merit (Z) is defined as follows:

$$Z = \frac{\alpha^2}{k\rho}, \quad (10)$$

where α is the Seebeck coefficient, ρ is the electrical resistivity, and k is the thermal conductivity. r is the thermal contact ratio, w is the ratio of ceramic thickness to the length of TE leg, and n is the electrical resistivity ratio. For the TE module adopted in the present work, $w = 0.516$. r and n are 0.2 and 0.1, respectively, which are widely used for TE modules with ceramic substrates and type-A configuration (Rowe and Gao, 1998). L is the length of TE leg. Temperature dependent properties (α, ρ, k, shown in Appendix A) were used to calculate Z. The ZT_{ave} value varies between 0.86 and 0.88, where $T_{ave} = 0.5(T_{\text{h}} + T_{\text{c}})$. The residence time ($\tau$) of flue gases is estimated as follows:

$$\tau = \frac{1000 A_{flue} L_{flue}}{Q_{flue}}, \quad (11)$$

where Q_{flue}, A_{flue}, and L_{flue} are the volume flow rate of flue gases, cross sectional area of flue gas channel, and flue gas channel length, respectively.

3. Results and discussions

3.1. Temperature profiles

Combustion temperatures under various input powers and equivalent ratios are shown in Fig. 3. A thermal image at $\varphi = 0.9$ with input power of 108 W is shown in Fig. 3(b). The combustion temperature was considerably high. For example, the combustion temperature was 1239 °C when the input power was 108 W at $\varphi = 0.9$. Thus, sustained combustion and high combustion efficiency can be ensured. The hot-end temperature was lower than 100 °C because of the heat adsorption of TE modules through copper-based combustion walls. The combustion temperature at $\varphi = 1.0$ was lower than those at $\varphi = 0.9$, indicating that the combustion efficiency at $\varphi = 0.9$ was higher than those at $\varphi = 1.0$. The thermal image showed that the entire MCP-TEG remained at low temperature level except the area near the flue gas spout because this area was difficult to wrap insulation materials. The thermal image was used to estimate the heat losses through convections and thermal radiations.

The hot-end temperatures and temperature differences under various load resistances at different input powers and equivalent ratios are shown in Fig. 4. Although the hot-end temperature was lower than 100 °C, temperature differences were large, and comparable to several previous studies (Vican et al., 2002; Federici et al., 2006; Yoshida et al., 2006; Singh et al., 2016; Shimokuri et al., 2015). For example, the highest hot-end temperature was 95 °C, and the corresponding temperature difference was 75 °C. The hot-end temperatures and temperature differences at $\varphi = 0.9$ were higher than those at $\varphi = 1.0$ under the same input power, which were caused by different combustion efficiencies. For example, the averaged hot-end temperatures and temperature differences of $P_{\text{in}} = 108$ W were 91.6 °C and 71.3 °C at $\varphi = 0.9$, whereas the averaged values were 82.9 °C and 61.6 °C at $\varphi = 1.0$ under the same input power.

The heat flow rate of flue gases can be obtained as follows:

$$P_{flue} = m_{flue} c_p (T_{\text{out}} - T_{\text{in}}) = 18.4 \text{ W}, \quad (12)$$

where T_{out} and T_{in} are direct measurements with thermocouples. For the experimental case at $P_{\text{in}} = 108$ W and $\varphi = 0.9$, $T_{\text{out}} = 346.3$ °C, $T_{\text{in}} = 19$ °C. m_{flue} is the mass flow rate (4.110^{-5} kg/s) of flue gases, which can be determined by the total mass flow rate of methane and air. As a result, the heat flow rate of flue gases was calculated to be 18.4 W, and it occupies 17.1% of the input power.

The natural convective heat transfer coefficient, h_{air}, is assumed to be 10 W/m^2 K for the insulation layer of the mesoscale combustor, and the corresponding emissivity was calibrated to be 0.6 with the IR camera and a type K thermocouple. Therefore, the heat losses through natural convections and thermal radiations are estimated as follows,

$$\begin{aligned} P_{conv} + P_{rad} &= h_{air} A_{\text{surf}} (T_{\text{surf}} - T_{\text{in}}) \\ &\quad + \varepsilon \sigma A_{\text{surf}} \left[(T_{surf} + 273)^4 - (T_{in} + 273)^4 \right] \\ &= 3.62 \text{ W} + 1.63 \text{ W} \\ &= 5.25 \text{ W}, \end{aligned} \quad (13)$$

where T_{surf} and A_{surf} are the outside surface temperature (77.5 °C) and area (0.00608 m^2) of the insulation layer. The convective heat loss is subjected to certain errors because the natural convective heat transfer coefficient lies between 5 and 15 W/m^2 K (Holman, 2008). Given the fact that the convective heat loss rate (3.62 W) occupies only 3.35% of the total input power (108 W), and that only 0.05% difference was obtained for the TE efficiency, this assumption is justified.

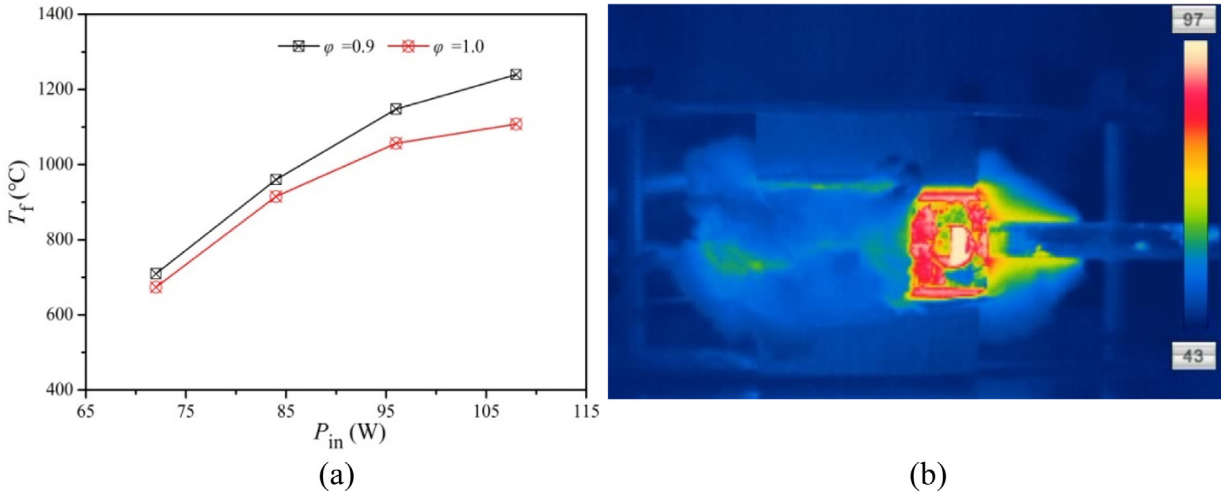

Fig. 3. Combustion temperature (a) and thermal image of the entire MCP-TEG (b).

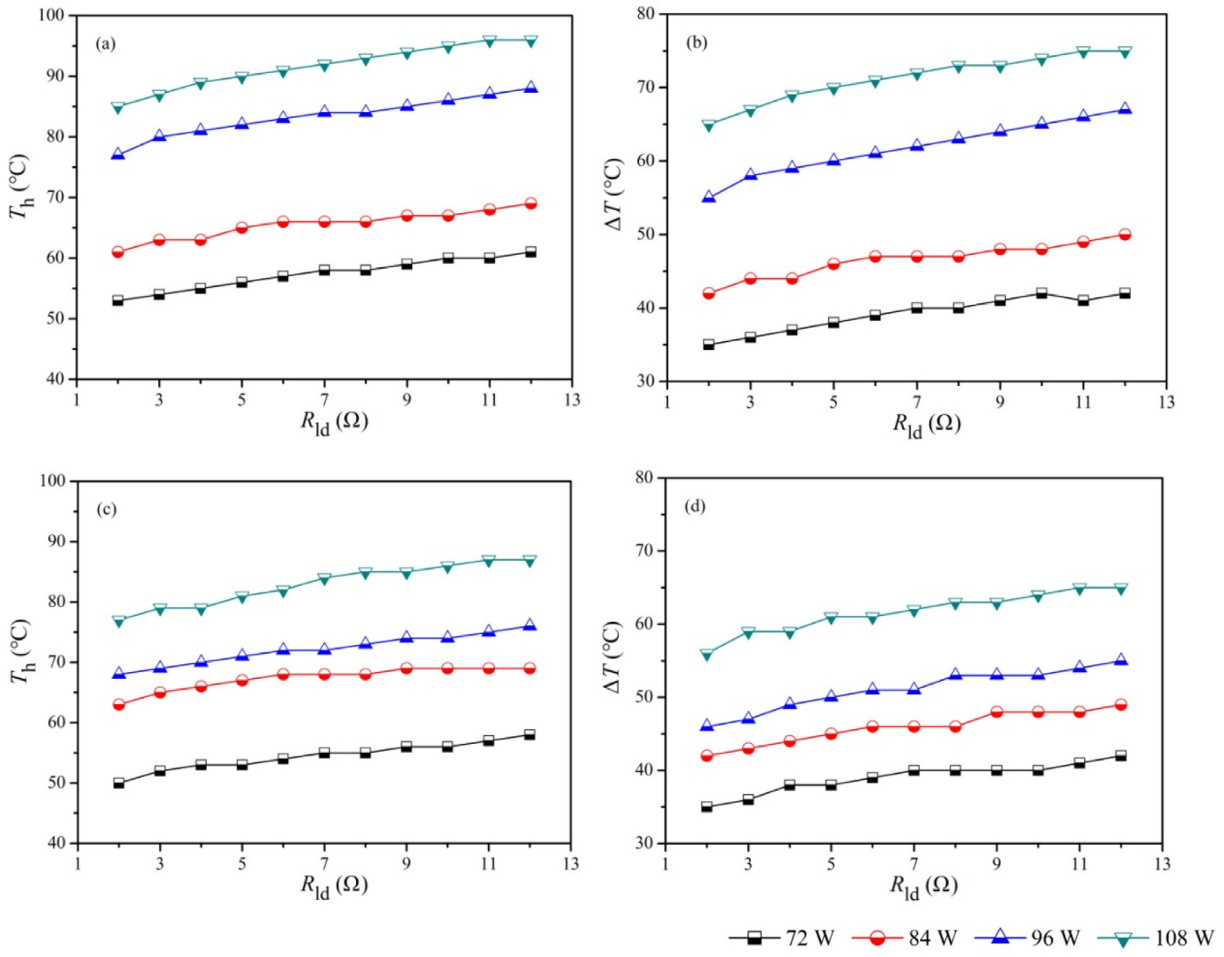

Fig. 4. Hot-end temperatures and temperature differences under various load resistances and input powers (a) T_h at $\varphi = 0.9$ (b) ΔT at $\varphi = 0.9$ (c) T_h at $\varphi = 1.0$ (d) ΔT at $\varphi = 1.0$.

3.2. Power load features

The load powers and corresponding voltages under various load resistances, input powers, and equivalent ratios are shown in Figs. 5 and 6. For the proposed MCP-TEG, lean combustion is required to obtain a good combustion performance. As shown in Fig. 5(a)–(b), the load powers at $\varphi = 0.9$ were higher than those at $\varphi = 1.0$. For example, the maximum load power was 1.88 W at $\varphi = 0.9$ when the input power was 108 W, whereas the maximum load power was 1.48 W at $\varphi = 1.0$ when the input power remained unchanged. This condition was caused by different combustion efficiencies at these equivalent ratios, which were directly proportional to the actual heat release rates. The load power decreased with the decrease of equivalent ratio to

0.8, which was caused by introducing too much diluent airs. Furthermore, the load resistance affects the load power significantly, which is controlled by the impedance matching principle. As a result, the increase of voltage shown in Fig. 6 is not necessary to generate a larger electric power than those cases with low voltages, and the increase of voltage with load resistance is due to the fact that the load resistance is connected in series to the internal resistance.

Voltage rapidly increased with the increase of load resistance. The voltage at $\varphi = 0.9$ was significantly larger than those at $\varphi = 1.0$ under the same input power. For example, the voltage at the maximum load power of 1.88 W was 4.33 V when $\varphi = 0.9$, whereas the voltage at the maximum load power of 1.48 W was 3.65 V when $\varphi = 1.0$. This phenomenon could be easily understood because voltage was directly proportional to temperature difference. An optimized combustion status released considerable heat to create a high temperature difference, which resulted in a large voltage, and augmented the load power. Thus, Figs. 4–6 validate each other.

3.3. Efficiencies

Overall efficiencies under various input powers and load resistances are shown in Fig. 7. Overall efficiencies at $\varphi = 0.9$ were slightly larger than those at $\varphi = 1.0$ when the input powers were low (72 W and 84 W). However, the difference of overall efficiency increased when the input power increased to 96 W and 108 W. For example, the largest overall efficiency at $\varphi = 0.9$ was 1.74% when the input power was 108 W, whereas the largest overall efficiency at $\varphi = 1.0$ was 1.37% when the input power remained unchanged.

The abovementioned phenomenon was caused by different combustion efficiencies, as shown in Fig. 8. Fig. 8(a) shows the heat collection efficiency, combustion efficiency, and estimated residence time (τ). Heat collection efficiency was calculated by estimating the heat flow rate of flue gases, and heat losses through convections and thermal radiations, as shown in Fig. 8(b). The combustion temperature increased with the increase of input power, which was beneficial for complete combustion. Thus, the combustion efficiency improved. For example, the combustion efficiency was 83.7% when the input power was 74 W, whereas it increased to 97.4% when the input power was 108 W. The residence time reduced by increasing the input power, which decreased from 134 ms to 60 ms when the input power was increased from 74 W to 108 W, resulting in different heat collection efficiencies. Heat collection efficiency decreased from 87.7% to 77.4% when the input power was increased from 74 W to 108 W. The increasing input power augmented the overall efficiency with moderate amplitude, as shown in Fig. 7. Heat losses through convections and thermal radiations cannot be ignored because the estimated heat loss ratio occupied approximately 5% in the present work. As shown in Fig. 8(b), the heat loss ratio slightly increased with the increase of input power.

The overall efficiency (1.74%) in the present study was comparable to previous studies (∼2%), as shown in Table 1. Detailed discussions related to comparisons with previous studies and possible insights were presented in the following section. The essential issues behind the overall efficiency were the TE efficiency and the gap between overall and TE efficiencies, which was controlled by Eq. (8), as shown in Fig. 9. The limit of overall efficiency was the TE efficiency. TE efficiency was controlled by the parameter of *ZT* value, which was fixed when using a particular TE material and working at a particular temperature. TE efficiency could be theoretically predicted using Eqs. (9)–(10). TE modules normally worked when the experimental TE efficiency was close to the theoretical prediction. As shown in Fig. 9(a), the experimental TE efficiency reached 91.4% on average of the theoretical prediction. Thus, the TE modules used in the present study normally worked. The ratio of overall efficiency to TE efficiency measures the performance of the entire MCP-TEG. As shown in Fig. 9(b), the ratio of overall efficiency to TE efficiency reaches 75.3%, which is higher than those in previous studies. Room for improvements remains, and a value of 90% should be targeted in future studies.

3.4. Discussions

Performance comparisons of various MCP-TEGs were shown in Fig. 10, which was based on the data in Table 1 and Eq. (8). In case that heat collection and combustion efficiencies were unreported, they were estimated to be 70% and 95% to deduce corresponding TE efficiencies in Fig. 10(b), and these assumptions were considerably high. It seems that notable progress was achieved in recent years because the overall efficiency of several MCP-TEGs (Yadav et al., 2015; Aravind et al., 2018b) reached 4.6%, which is shown in Fig. 10(a). However, the limit of overall efficiency was the TE efficiency according to Eq. (8), and this limit could be only reached with complete combustion ($\eta_{\text{fuel}} = 100\%$) and heat collection ($\eta_{\text{heat}} = 100\%$). Unfortunately, complete combustion and heat collection are unlikely to obtain.

The power of Eq. (8) can be revealed by deducing the TE efficiency, as shown in Fig. 10(b). Several deduced TE efficiencies were significantly larger than 10% for Bi_2Te_3 based TE modules, which implies that these works need further confirmations because the TE efficiency of Bi_2Te_3 based TE module is only several percentages (∼5%) (Hu et al., 2016; Liu et al., 2018). This analysis also revealed that combustion and heat collection have to be simultaneously optimized to augment the overall efficiency, otherwise other TE materials with large *ZT* value should be used (Zhao et al., 2014c).

An effective way to the ratio of overall efficiency to TE efficiency is revealed, that is, incorporating a proper mesoscale combustor to improve the combustion process and designing serpentine channels to enhance the heat recovery from flue gases. As presented in the above experimental results, the maximum overall efficiency is 1.74% and the corresponding TE efficiency is 2.31%. This finding corresponds to 24.7% reduction of TE efficiency. This reduction is mainly caused by the heat collection efficiency of 77.4% because the combustion efficiency is as high as 97.4%. Nevertheless, the obtained heat collection efficiency is substantial high compared to previous works, which is shown in Table 1. Residence time is an essential parameter behind the heat collection efficiency, and it was measured to be 60 ms when the input power is 108 W at $\varphi = 0.9$. The residence time is comparable to previous studies, such as 50–60 ms in Vican's work (Vican et al., 2002), 40–120 ms in Yoshida's work (Yoshida et al., 2006), and 10–50 ms in Shimokuri's work (Shimokuri et al., 2015, 2017). Thus, increasing the ratio of flue gas channel length to channel hydraulic diameter is beneficial to increase the residence time of flue gases so as to enhance the heat collection, and finally improves the overall efficiency. The pressure drop, which was not measured and discussed in the present work, should be considered to balance the air supply in field applications. Furthermore, a substantial high overall efficiency (1.74%) was obtained in the present MCP-TEG compared to previous reports at a low hot-end temperature (95 °C), which is lower than those in previous works. This ensures the long-running service of the present MCP-TEG and the low thermal signature.

Only 1–2 ppm NO was detected in the flue gases. However, this finding was small considering the accuracy of the NO sensor of 5 ppm. CO emission was considerable, which decreased from 3811 ppm at 72 W to 749 ppm at 108 W when the equivalent

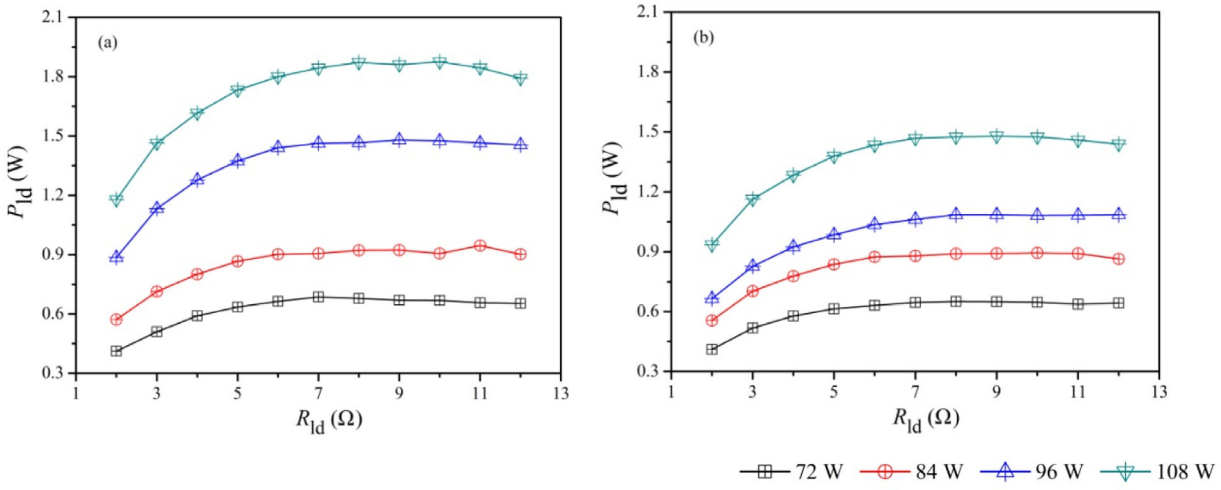

Fig. 5. Load powers of MCP-TEG under various load resistances and input powers (a) $\varphi = 0.9$ (b) $\varphi = 1.0$.

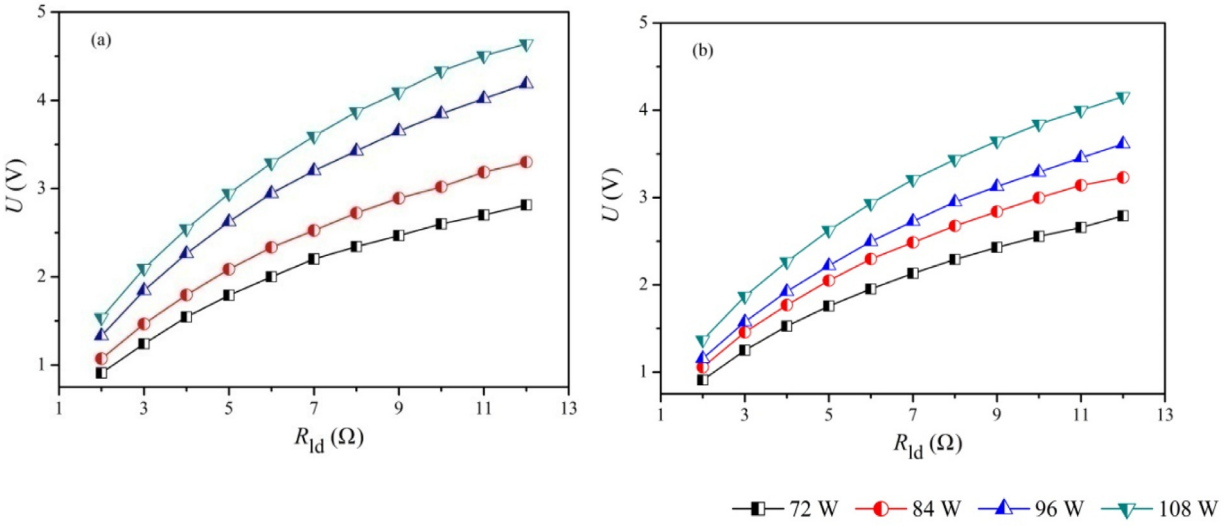

Fig. 6. Voltages of MCP-TEG under various load resistances and input powers (a) $\varphi = 0.9$ (b) $\varphi = 1.0$.

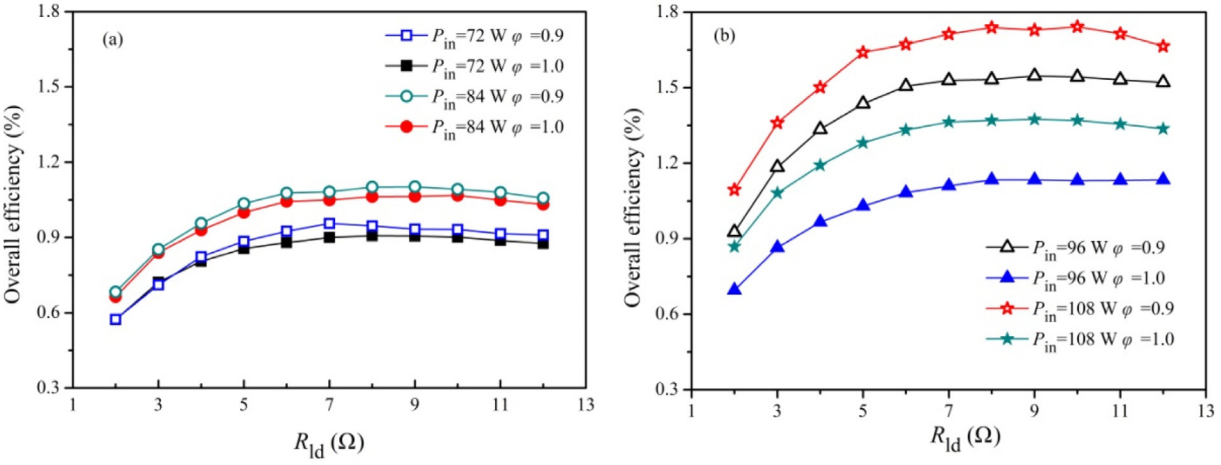

Fig. 7. Overall efficiencies of MCP-TEG under various load resistances and input powers (a) $P_{in} = 72$ W and $P_{in} = 84$ W. (b) $P_{in} = 96$ W and $P_{in} = 108$ W.

ratio was 0.9. However, CO emission remained in the ppm range, indicating that its influence on the calculation of combustion efficiency was limited. The threat of CO to human health must be considered in field applications. CO emission was consistent

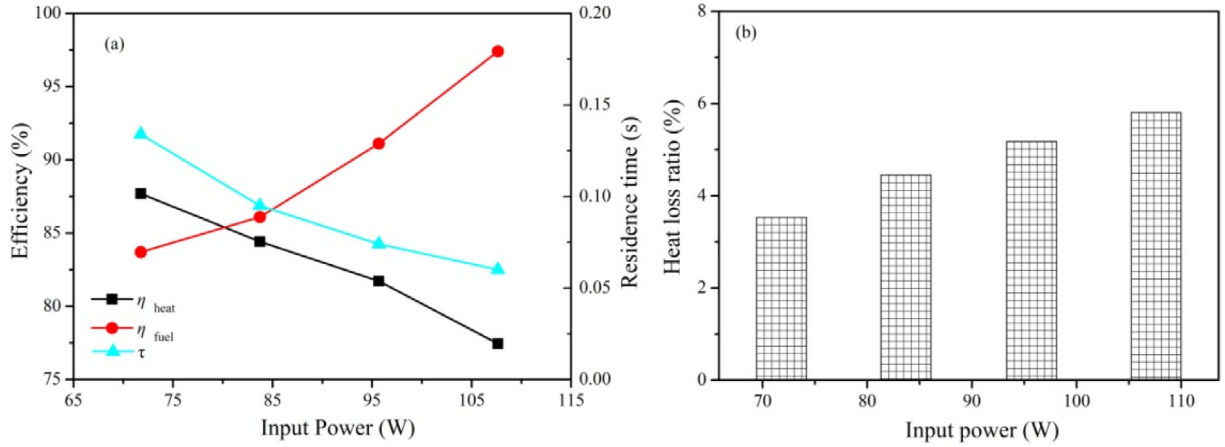

Fig. 8. Influences of input power on (a) heat collection efficiency, combustion efficiency, flue gas residence time, and (b) heat loss ratio through convections and thermal radiations when $\varphi = 0.9$.

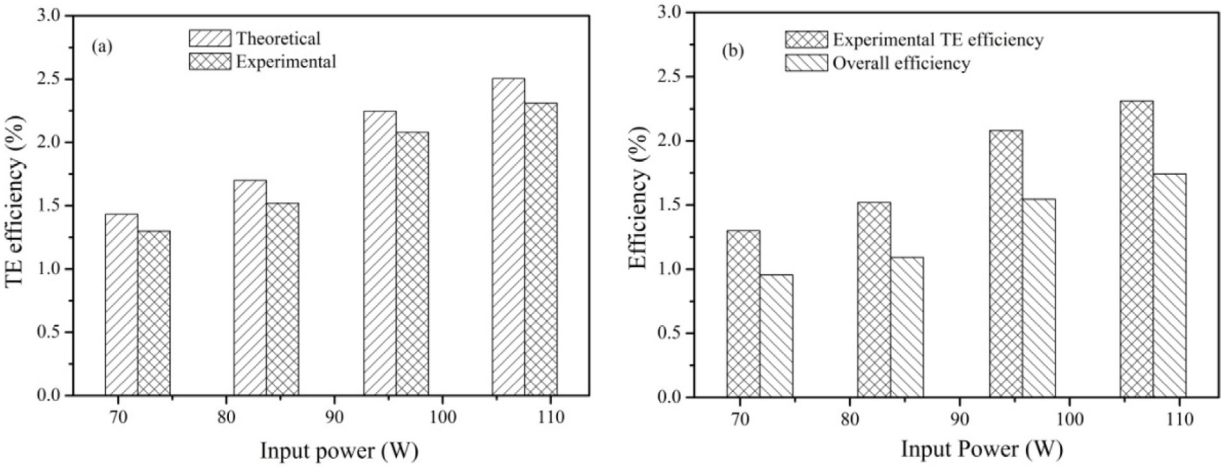

Fig. 9. TE and overall efficiencies at maximum electric power conditions when $\varphi = 0.9$ (a) comparisons of TE efficiency between experimental data and theoretical predictions (b) comparisons between experimental TE and overall efficiencies.

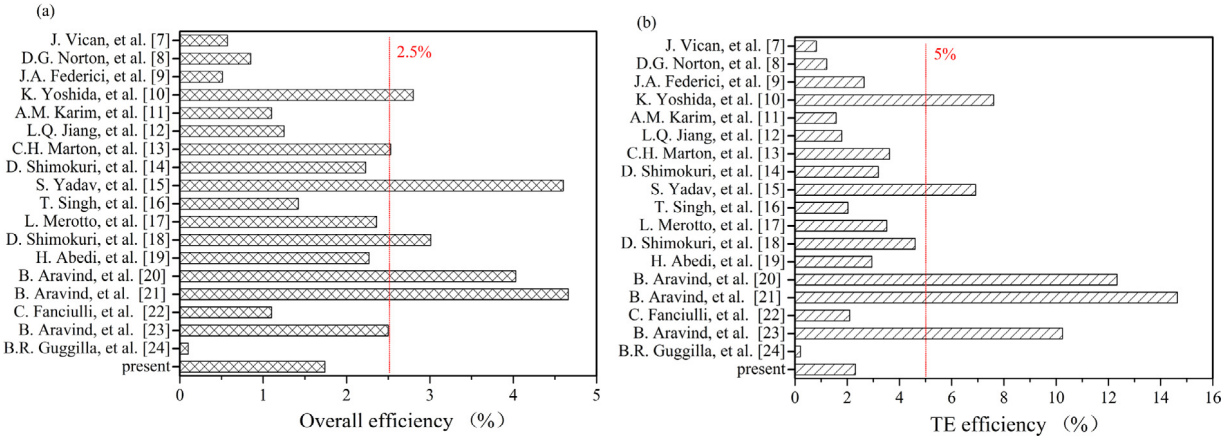

Fig. 10. Performance comparisons of various MCP-TEGs (a) overall efficiency (b) deduced TE efficiency.

with previous studies (Jiang et al., 2011; Abedi et al., 2017; Fanciulli et al., 2018), and this problem should be focused in future investigations.

4. Conclusions

An MCP-TEG was presented in this study. The MCP-TEG worked with input powers between 72 W and 108 W, and generated a maximum electric power of 1.88 W with an overall

efficiency of 1.74%. The outside surface temperature of the MCP-TEG was lower than 100 °C. The heat collection efficiency is 77.4%, which augments the ratio of overall efficiency to TE efficiency reaching 75.3%. Besides, heat losses through nature convections and thermal radiations occupied approximately 5% of the input power. Thus, heat losses cannot be ignored in future studies.

The relationship ($\eta_{sys} = \eta_{fuel}\eta_{heat}\eta_{TE}$) among overall, combustion, heat collection and TE efficiencies was developed. The limit of the overall efficiency of an MCP-TEG is the TE efficiency. An effective metrics to evaluate the MCP-TEG performance should be the ratio of overall efficiency to TE efficiency (η_{sys}/η_{TE}) at the desired hot-end and cold-end temperatures. The gap between the overall and TE efficiencies was mainly determined by combustion and heat collection efficiencies. Increasing the ratio of flue gas channel length to channel hydraulic diameter is an effective way to increase the residence time of flue gases, which improves the overall efficiency.

Declaration of competing interest

The authors declare that they have no known competing financial interests or personal relationships that could have appeared to influence the work reported in this paper.

CRediT authorship contribution statement

Hanming Gao: Conceptualization, Validation, Investigation. **Guoneng Li:** Conceptualization, Funding acquisition, Investigation, Writing - original draft, Writing - review & editing. **Wei Ji:** Funding acquisition. **Dongya Zhu:** Data curation, Investigation. **Youqu Zheng:** Validation, Methodology. **Feixing Ye:** Writing - original draft, Writing - review & editing. **Wenwen Guo:** Data curation.

Acknowledgments

This work was supported by the key R&D plan of Zhejiang Province, China (Grant no. 2020C03115), National Natural Science Foundation of China (Grant nos. 51906220 and 51476145), and the Natural Science Foundation of Zhengjiang Province, China (Grant no. LQ19E060002).

Appendix A

The physical properties of TE material are temperature-dependent based on the datasheets provided by manufacturer. Three-order polynomial fittings are applied, and the results are expressed as follows:

$$k_p(T) = tp_1 + tp_2T + tp_3T^2 + tp_4T^3, \quad (A.1)$$

$$k_n(T) = tn_1 + tn_2T + tn_3T^2 + tn_4T^3, \quad (A.2)$$

$$\rho_p(T) = ep_1 + ep_2T + ep_3T^2 + ep_4T^3, \quad (A.3)$$

$$\rho_n(T) = en_1 + en_2T + en_3T^2 + en_4T^3, \quad (A.4)$$

$$\alpha_p(T) = sp_1 + sp_2T + sp_3T^2 + sp_4T^3, \quad (A.5)$$

$$\alpha_n(T) = sn_1 + sn_2T + sn_3T^2 + sn_4T^3, \quad (A.6)$$

where k, ρ, and α are thermal conductivity, electrical resistivity, and Seebeck coefficient, respectively. T is the temperature. Subscripts p and n denote the P-type and N-type legs, respectively. The constants are as follows:

$tp_1 = 4.389$, $tp_2 = -1.8168 \times 10^{-2}$, $tp_3 = 2.437956 \times 10^{-5}$,
$tp_4 = 4.793196 \times 10^{-10}$;
$tn_1 = 4.09878$, $tn_2 = -1.4976 \times 10^{-2}$, $tn_3 = 1.799196 \times 10^{-5}$,
$tn_4 = 1.692996 \times 10^{-9}$;
$ep_1 = -6.7074 \times 10^{-6}$, $ep_2 = 5.09 \times 10^{-8}$,
$ep_3 = 6.33243 \times 10^{-11}$, $ep_4 = -5.31761 \times 10^{-14}$;
$en_1 = -1.51744 \times 10^{-5}$, $en_2 = 1.142 \times 10^{-7}$,
$en_3 = -8.17056 \times 10^{-11}$, $en_4 = -5.18487 \times 10^{-15}$;
$sp_1 = -1.0915819 \times 10^{-4}$, $sp_2 = 1.67585 \times 10^{-6}$,
$sp_3 = -2.12 \times 10^{-9}$, $sp_4 = 4.43743 \times 10^{-14}$;
$sn_1 = -4.3833365 \times 10^{-4}$, $sn_2 = 2.90422 \times 10^{-6}$,
$sn_3 = -9.76 \times 10^{-9}$, $sn_4 = 1.01202 \times 10^{-11}$.

References

Abedi, H., Merotto, L., Fanciulli, C., Dondè, R., Iuliis, S.D., Passaretti, F., 2017. Study of the performances of a thermoelectric generator based on a catalytic meso-scale H_2/C_3H_8 fueled combustor. J. Nanosci. Nanotechnol. (17), 1592–1600.

Aravind, B., Khandelwal, B., Kumara, S., 2018a. Experimental investigations on a new high intensity dual microcombustor based thermoelectric micropower generator. Appl. Energy (228), 1173–1181.

Aravind, B., Raghuram, G.K.S., Kishore, V.R., Kumar, S., 2018b. Compact design of planar stepped micro combustor for portable thermoelectric power generation. Energy Convers. Manage. (156), 224–234.

Aravind, B., Saini, D.K., Kumar, S., 2019. Experimental investigations on the role of various heat sinks in developing an efficient combustion based micro power generator. Appl. Therm. Eng. (148), 22–32.

Champier, D., Bédécarrats, J.P., Kousksou, T., Rivaletto, M., Strub, F., Pignolet, P., 2011. Study of a TE (thermoelectric) generator incorporated in a multifunction wood stove. Energy (36), 1518–1526.

Chou, S.K., Yang, W.M., Chua, K.J., Li, J., Zhang, K.L., 2011. Development of micro power generators – A review. Appl. Energy (88), 1–16.

Essig, S., Steiner, M.A., Allebé, C., Geisz, J.F., Paviet-Salomon, B., Ward, S., Descoeudres, A., LaSalvia, V., Barraud, L., Badel, N., Faes, A., Levrat, J., Despeisse, M., Ballif, C., Stradins, P., Young, D.L., 2016. Realization of GaInP/Si dual-junction solar cells with 29.8% 1-sun efficiency. IEEE J. Photovolt. (6), 1012–1029.

Fanciulli, C., Abedi, H., Merotto, L., Dondè, R., De Iuliis, S., Passaretti, F., 2018. Portable thermoelectric power generation based on catalytic combustor for low power electronic equipment. Appl. Energy (215), 300–308.

Federici, J.A., Norton, D.G., Bruggemann, T., Voit, K.W., Wetzel, E.D., Vlachos, D.G., 2006. Catalytic microcombustors with integrated thermoelectric elements for portable power production. J. Power Sources (161), 1469–1478.

Guggilla, B.R., Alexander, R., Bakrania, S., 2019. Platinum nanoparticle catalysis of methanol for thermoelectric power generation. Appl. Energy (237), 155–162.

Holman, J.P., 2008. Heat Transfer, tenth ed. Mc Graw Hill, USA, pp. 327–347, Chapter 7.

Hu, X., Jood, P., Ohta, M., Kunii, M., Nagase, K., Nishiate, H., Kanatzidis, M.G., Yamamoto, A., 2016. Power generation from nanostructured PbTe-based thermoelectric: comprehensive development from materials to modules. Energy Environ. Sci. (9), 517–529.

Jiang, L.Q., Zhao, D.Q., Guo, C.M., Wang, X.H., 2011. Experimental study of a plat-flame micro combustor burning DME for thermoelectric power generation. Energy Convers. Manage. (52), 596–602.

Karim, A.M., Federici, J.A., Vlachos, D.G., 2008. Portable power production from methanol in an integrated thermoeletric/microreactor system. J. Power Sources (179), 113–120.

Li, G.N., Zhang, S., Zheng, Y.Q., Zhu, L.Y., Guo, W.W., 2018. Experimental study on a stove-powered thermoelectric generator (STEG) with self starting fan cooling. Renew. Energy (121), 502–512.

Liu, Z., Mao, J., Sui, J., Ren, Z., 2018. High thermoelectric performance of α-MgAgSb for power generation. Energy Environ. Sci. (11), 23–44.

Marton, C.H., Haldeman, G.S., Jensen, K.F., 2011. Portable thermoelectric power generator based on a microfabricated silicon combustor with low resistance to flow. Ind. Eng. Chem. Res. (50), 8468–8475.

Merotto, L., Fanciulli, C., Dondè, R., Iuliis, S.D., 2016. Study of a thermoelectric generator based on a catalytic premixed meso-scale combustor. Appl. Energy (162), 346–353.

Montecucco, A., Siviter, J., Knox, A.R., 2017. Combined heat and power system for stoves with thermoelectric generators. Appl. Energy (185), 1336–1342.

Mustafa, K.F., Abdullah, S., Abdullah, M.Z., Sopian, K., 2017. A review of combustion-driven thermoelectric (TE) and thermophotovoltaic (TPV) power systems. Renew. Sustain. Energy Rev. (71), 572–584.

Najjar, Y.S.H., Kseibi, M., 2017. Evaluation of experimental JUST thermoelectric stove for electricity-deprived regions. Renew. Sustain. Energy Rev. (69), 854–861.

Norton, D.G., Voit, K.W., Brüggemann, T., Vlachos, D.G., Portable power generation via integrated catalytic microcombustion-thermoelectric devices. In: Proceedings for the Army Science Conference (24th), 2005, Nov 29 – Dec 2, Orlando, Florida.

Nuwayhid, R.Y., Shihadeh, A., Ghaddar, N., 2005. Development and testing of a domestic woodstove thermoelectric generator with natural convection cooling. Energy Convers. Manage. 46, 1631–1643.

O'Shaughnessy, S.M., Deasy, M.J., Doyle, J.V., Robinson, A.J., 2015. Performance analysis of a prototype small scale electricity-producing biomass cooking stove. Appl. Energy (156), 566–576.

Rowe, D.M., 1995. CRC Handbook of Thermoelectrics. CRC press, London, chapter 19, chapter 38 and chapter 44.

Rowe, D.M., Gao, M., 1998. Evaluation of thermoelectric modules for power generation. J. Power Sources (73), 193–198.

Shimokuri, D., Hara, T., Matsumoto, R., 2015. Development of a small-scale power system with meso-scale vortex combustor and thermo-electric device. J. Micromech. Microeng. (25), 104004.

Shimokuri, D., Taomoto, Y., Matsumoto, R., 2017. Development of a powerful miniature power system with a meso-scale vortex combustor. Proc. Combust. Inst. (36), 4253–4260.

Singh, T., Marsh, R., Min, G., 2016. Development and investigation of a non-catalytic self-aspirating meso-scale premixed burner integrated thermoelectric power generator. Energy Convers. Manage. (117), 431–441.

Sonoc, A., Jeswiet, J., Soo, V.K., 2015. Opportunities to improve recycling of automotive lithium ion batteries. Proc. CIRR (29), 752–757.

Sornek, K., Filipowicz, M., Żołądek, M., Kot, R., Mikrut, M., 2019. Comparative analysis of selected thermoelectric generators operating with wood-fired stove. Energy (166), 1303–1313.

Vican, J., Gajdeczko, B.F., Dryer, F.L., Milius, D.L., Aksay, I.A., Yetter, R.A., 2002. Development of a microreactor as a thermal source for microelectromechanical systems power generation. Proc. Combust. Inst. (29), 909–916.

Xiao, G., Yang, T., Liu, H., Ni, D., Ferrari, M.L., Li, M., Luo, Z., Cen, K., Ni, M., 2017. Recuperators for micro gas turbines: A review. Appl. Energy (197), 83–99.

Yadav, S., Yamasani, P., Kumar, S., 2015. Experimental studies on a micro power generator using thermo-electric modules mounted on a micro-combustor. Energy Convers. Manage. (99), 1–7.

Yoshida, K., Tanaka, S., Tomonari, S., Satoh, D., Esashi, M., 2006. High-energy density miniature thermoelectric generator using catalytic combustion. J. Microelectromech. Syst. (15), 195–203.

Zhang, T., Wang, P., Chen, H., Pei, P., 2018. A review of automotive proton exchange membrane fuel cell degradation under start-stop operating condition. Appl. Energy (223), 249–262.

Zhao, D., Ega, E., 2014. Energy harvesting from self-sustained aeroelastic limit cycle oscillations of rectangular wings. Appl. Phys. Lett. (105), 103903.

Zhao, D., Ji, C., Li, S., Li, J., 2014a. Thermodynamic measurement and analysis of dual-temperature thermoacoustic oscillations for energy harvesting application. Energy (65), 517–526.

Zhao, D., Ji, C., Teo, C., Li, S., 2014b. Performance of small-scale bladeless electromagnetic energy harvesters driven by water or air. Energy (74), 99–108.

Zhao, L., Lo, S.H., Zhang, Y., Sun, H., Tan, G., Uher, C., Wolverton, C., Dravid, V.P., Kanatzidis, M.G., 2014c. Ultralow thermal conductivity and high thermoelectric figure of merit in SnSe crystals. Nature (508), 373–377.